

Emergence of a Landau level structure in dark optical lattices

Sylvain Nascimbene* and Jean Dalibard†

Laboratoire Kastler Brossel, Collège de France, CNRS, ENS-PSL University,
Sorbonne Université, 11 Place Marcelin Berthelot, 75005 Paris, France

(Dated: December 20, 2024)

An optical flux lattice is a set of light beams that couple different internal states of an atom, thereby producing topological energy bands. Here we present a configuration in which the atoms exhibit a dark state, i.e. an internal state that is not coupled to the light. At large light intensity, the low-energy dynamics is restricted to the dark state, leading to an effective continuum model with a Landau-level-like structure. This structure is dramatically different from that of usual topological optical lattices, which lead to discrete models in the tight-binding limit. The proposed system is essentially immune to heating due to photon scattering, making it a highly promising way to emulate the integer or fractional quantum Hall effect.

The generation of topological bands for atoms or photons moving in a periodic potential has been recently the subject of many theoretical and experimental studies (for reviews, see e.g. [1, 2]). It opens the way to a simulation of the quantum Hall effect, from the integer to the fractional regimes when the role of interactions increases. Among the various schemes that have been considered for atoms moving in a laser field, optical flux lattices (OFL) have the advantage of not requiring any time modulated parameters (which may lead to undesired heating), while providing a large flux density, typically one or two flux quanta per unit cell [3]. However, OFL tend to require relatively complex laser beam structures, when they are aimed at atomic species, such as alkali-metal atoms, commonly used in quantum gas experiments [4, 5]. In addition, OFL schemes proposed so far may induce significant photon scattering, which limits the available time during which the atomic gas remains cold enough to observe topology-induced effects.

In this paper, we propose a modified version of the optical lattice concept, which can operate with a so-called ‘dark state’, thus reducing considerably the heating problem due to photon scattering. The energy spectrum generated by our scheme is remarkably close to the Landau level structure for a charged particle in a uniform magnetic field. For realistic parameters, we obtain a series of many equidistant, non-overlapping, topological bands, each with a Chern index equal to 1. Being restricted to the dark internal state, the atoms remain weakly coupled to light, giving rise to delocalized orbitals. This behavior contrasts with other realizations of topological bands in optical lattices, which can be described by discrete lattice models such as the Haldane and Harper-Hofstadter models [6–8]. As an illustration of the topological character of the bands, we check that an ideal Fermi gas populating the ground band should exhibit an incompressible bulk surrounded by chiral edge states, and interacting bosons should organize themselves into an ordered vortex lattice.

The atom-laser coupling. We consider atoms with an electronic ground level g with angular momentum $J_g = 1$, moving in the xy plane. The laser beams form-

ing the OFL are supposed to be monochromatic and they couple the ground level g to an excited level e , also with angular momentum $J_e = 1$. One can then identify a space-dependent dark state, linear combination of $|g, m_z = \pm 1\rangle$, where m_z labels the projection of the internal angular momentum along z [9].

Since the polarization vector $\boldsymbol{\epsilon}(\mathbf{r})$ lies in the xy plane, it can be decomposed at any point \mathbf{r} on the circular polarization basis $\boldsymbol{\epsilon}_\pm$, $\boldsymbol{\epsilon}(\mathbf{r}) \propto \alpha_+(\mathbf{r})\boldsymbol{\epsilon}_+ + \alpha_-(\mathbf{r})\boldsymbol{\epsilon}_-$, where $\alpha_\pm(\mathbf{r})$ are complex, spatially periodic functions. The atom-laser coupling reads in the $|g, \pm 1\rangle$ basis:

$$\hat{V}(\mathbf{r}) = V_0 \begin{pmatrix} |\alpha_-|^2 & -\alpha_+\alpha_-^* \\ -\alpha_+^*\alpha_- & |\alpha_+|^2 \end{pmatrix}, \quad (1)$$

where V_0 is a real, positive energy. Here we restricted the internal atomic dynamics to the Λ system formed by $\{|g, \pm 1\rangle, |e, 0\rangle\}$, and we adiabatically eliminated the excited state $|e, 0\rangle$ assuming that the positive detuning from resonance is large compared to the Rabi frequency characterizing the atom-laser coupling (see appendix 1 for details) [10].

The dark state $|\mathcal{D}(\mathbf{r})\rangle \propto \alpha_+(\mathbf{r})|g, +1\rangle + \alpha_-(\mathbf{r})|g, -1\rangle$ is the eigenstate of \hat{V} with energy 0, which provides a one-to-one correspondence between the Poincaré sphere for the polarization, and the Bloch sphere for the two-level system $|g, \pm 1\rangle$. The other eigenstate of \hat{V} is the bright state $|\mathcal{B}(\mathbf{r})\rangle \propto \alpha_-^*(\mathbf{r})|g, +1\rangle - \alpha_+^*(\mathbf{r})|g, -1\rangle$. Its energy $E_{\text{bright}}(\mathbf{r}) = V_0(|\alpha_+(\mathbf{r})|^2 + |\alpha_-(\mathbf{r})|^2)$ is positive everywhere so that the dark state is always the local ground state of the atom.

In this work, we will choose the following expressions for the coefficients $\alpha_\pm(\mathbf{r})$:

$$\alpha_+(\mathbf{r}) = 1 + \frac{1}{2} [\cos(kx) + \cos(ky)], \quad (2)$$

$$\alpha_-(\mathbf{r}) = \sin \left[\frac{k}{2}(x-y) \right] - i \sin \left[\frac{k}{2}(x+y) \right]. \quad (3)$$

The light-shift coupling is invariant upon discrete symmetries that combine discrete translations by $d\mathbf{e}_x$ or $d\mathbf{e}_y$ and the spin rotation $\hat{\sigma}_z$, where $d = 2\pi/k$, which allows us to define a square $d \times d$ unit cell.

The main results of this paper are based on the numerical calculation of the energy bands and of the associated Bloch states for a two-level atom moving in the potential $V(\mathbf{r})$. This will be done without any assumption regarding the adiabatic following of the dark state. However, it is interesting to start with the case when this adiabatic following is assumed. A first remark is that the dark state wraps the Bloch sphere, which is a necessary condition for the operation of an OFL. For example, the north pole $|g, +1\rangle$ is reached when $\mathbf{r} \rightarrow \mathbf{0}$, and the south pole $|g, -1\rangle$ when $\mathbf{r} \rightarrow (d/2, d/2)$. A consequence of this wrapping is that the flux across the unit cell of the synthetic magnetic field associated with the adiabatic following of the dark state $|\mathcal{D}(\mathbf{r})\rangle$ is nonzero. It is equal to $2\pi\hbar$, corresponding to one flux quantum across the unit cell.

This non-zero flux is one of the requirements for an OFL. Another requirement formulated in [3] is that the eigenstates of the coupling $V(\mathbf{r})$ should be non-degenerate at any point \mathbf{r} . This second requirement is clearly not fulfilled for the choice (3) since \hat{V} vanishes when $\mathbf{r} \rightarrow (d/2, d/2)$. In fact, this second requirement cannot be satisfied for a dark-state based OFL, as shown in appendix 2. However, as we see below, this does not prevent us to reach well separated topological bands.

Band structure. We show in Fig. 1a the band spectrum for a two-level atom for the Hamiltonian $\hat{p}^2/(2m) + \hat{V}(\mathbf{r})$ as a function of the light coupling amplitude V_0 . Here, energies are expressed in units of the cyclotron frequency $\hbar\omega_c = 2\pi\hbar^2/(md^2)$ expected for a Landau level with the same magnetic flux density as our OFL. For large couplings $V_0 \gg \hbar\omega_c$, we find a series of narrow energy bands at low energy, with an almost uniform spacing matching the cyclotron gap $\hbar\omega_c$. These bands essentially populate the dark state, with a very small residual light shift, shown in Fig. 1b for $V_0 = 100\hbar\omega_c$. For this light coupling, the ground band exhibits a width $\simeq 0.11\hbar\omega_c$ (about 7.2 times smaller than the gap to the first excited band), and the mean light shift is as low as $\langle\hat{V}\rangle \simeq 10^{-4}V_0$. The mixing between dark and bright states occurs at a higher energy, which can be estimated by computing the spectrum of an atom subjected to the lattice potential given by the position-dependent bright-state energy $E_{\text{bright}}(\mathbf{r})$. In the large depth limit, one can neglect tunneling between the different wells of the bright-state lattice, and one expects a harmonic spectrum for that state of frequency $\Omega_{\text{bright}} = \sqrt{2\pi V_0 \omega_c / \hbar}$ (dashed red lines in Fig. 1a).

To characterize the topological nature of the bands, we compute their Chern number, and find the value $C = 1$ for the first 19 bands at $V_0 = 100\hbar\omega_c$, confirming the similarity with Landau levels. Furthermore, the Berry curvature of the ground band is relatively uniform, with an rms deviation equal to $\simeq 25\%$ of its mean value.

Recent theoretical developments put forward a class of ‘ideal’ Chern bands, which share the same algebraic structure as Landau levels despite a non-uniform Berry

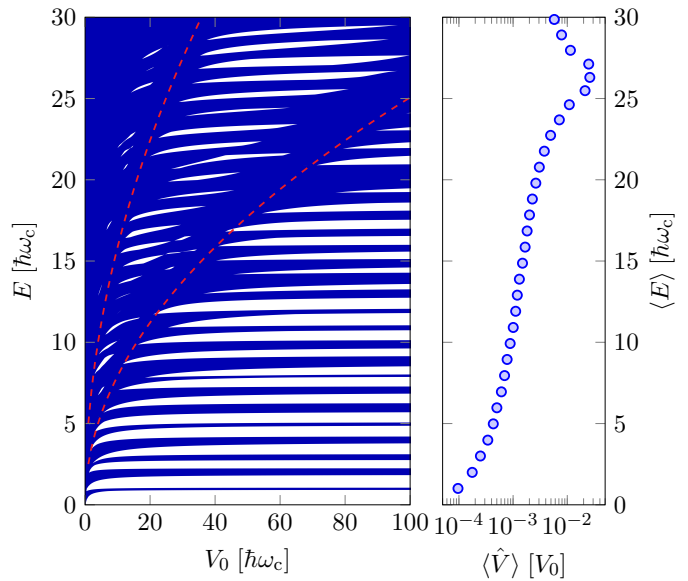


FIG. 1. (a) Band spectrum of the flux lattice as a function of the light coupling amplitude V_0 . In the regime $V_0 \gg \hbar\omega_c$, we find at low energy a succession of narrow energy bands with dominant dark-state character and an almost uniform spacing $\simeq \hbar\omega_c$. The red lines give a rough estimate of the first two bands with dominant bright-state character. They correspond to the energy levels $(n+1)\hbar\Omega_{\text{bright}}$ (with n integer) in the lattice potential experienced by the bright state in the large depth limit of independent harmonic wells. (b) Mean value $\langle\hat{V}\rangle$ of the light shift as a function of the mean total energy $\langle E \rangle$, averaged over the quasi-momentum \mathbf{q} , for the successive bands. The small value of the light shift for the low-energy bands shows that they predominantly populate the dark state.

curvature [11–14]. These bands are characterized by a quantum geometrical tensor $[\mathcal{Q}_{\mathbf{q}}]$ exhibiting a constant null vector \mathbf{w} , i.e. $[\mathcal{Q}_{\mathbf{q}}]\mathbf{w} = \mathbf{0}$ for all \mathbf{q} [12]. For the ground band of our OFL, we find that the circular vector $\mathbf{w} = \boldsymbol{\epsilon}_-$ acts as a null vector to a very good approximation (on average over the band, we find $\|[\mathcal{Q}_{\mathbf{q}}]\boldsymbol{\epsilon}_-\| = 0.06\|[\mathcal{Q}_{\mathbf{q}}]\boldsymbol{\epsilon}_+\|$). Consequently, the dynamics of the momentum component $q_x - iq_y$ is effectively suppressed, giving rise to momentum-space holomorphicity, akin to Landau levels.

Connection with Landau level orbitals. We can extend the comparison between the OFL and Landau levels by inspecting individual Bloch states in real space.

We first recall the Landau level formalism in a way that is well suited for comparison with flux lattices, i.e. a spatially periodic problem. We focus here on the ground band, the lowest Landau level (LLL). We assume a magnetic field $\mathbf{B} = B\mathbf{e}_z$ and adopt the Landau gauge $\mathbf{A} = -By\mathbf{e}_x$, for which the system is invariant upon x -translations $t_x(d_x) = \exp(-d_x\partial_x)$ of arbitrary distance d_x . The resulting conservation of the canonical momen-

tum p_x yields the LLL basis states $|\phi_{p_x}\rangle$, of wavefunction

$$\phi_{p_x}(x, y) = \frac{e^{ip_x x/\hbar}}{\pi^{1/4}\sqrt{\ell}} \exp\left[-\frac{(y - p_x\ell^2/\hbar)^2}{2\ell^2}\right],$$

where $\ell = \sqrt{\hbar/qB}$ is the magnetic length. The basis of $|\phi_{p_x}\rangle$ is not convenient for comparison with OFL Bloch bands, which are indexed by a 2D quasi-momentum \mathbf{q} . In order to symmetrize the x and y directions, we use another symmetry of the system, namely the y -magnetic translation symmetry $t_y(d_y) = \exp[-d_y(\partial_y - ix/\ell^2)]$ [15]. The commutation of translation symmetries obeys the algebra $t_x(d_x)t_y(d_y) = e^{-id_x d_y/\ell^2} t_y(d_y)t_x(d_x)$, hence a common basis of x - and y -translations can be found by choosing $d_x = d_y = d = \sqrt{2\pi}\ell$, such that the $d \times d$ unit cell is threaded by a single unit of magnetic flux quantum $\Phi_0 = h/q$. Magnetic Bloch states $|\psi_{q_x, q_y}\rangle$ invariant under both $t_x(d)$ and $t_y(d)$ can be formed by discrete sum of momentum states $|\phi_{p_x}\rangle$, as

$$|\psi_{q_x, q_y}\rangle = \sqrt{d} \sum_{n=-\infty}^{\infty} e^{iq_y d n} |\phi_{q_x + nQ}\rangle.$$

This expression corresponds to a discrete Fourier transform of all the momentum states $|\phi_{q_x + nQ}\rangle$ whose density probabilities are shifted one to the other along y by integer multiples of d . The states $|\psi_{q_x, q_y}\rangle$, defined in the Brillouin zone $|q_x|, |q_y| < \pi/d$, form a basis of the LLL. We note that the wavefunctions match the well-known LLL states defined on a torus of area $d \times d$ threaded by magnetic fluxes $2\pi(\Phi_x, \Phi_y)/\Phi_0 = (q_x, q_y)d$, given by [16]

$$\psi_{q_x, q_y}(x, y) = \frac{e^{-y^2/(2\ell^2) - iq_x q_y d^2/(2\pi)}}{\pi^{1/4}\sqrt{\ell}} \Theta \left[\begin{matrix} q_x d \\ q_y d \end{matrix} \middle| \begin{matrix} x - iy \\ d \end{matrix} \right],$$

where $\Theta[\begin{smallmatrix} g \\ b \end{smallmatrix}](z|\tau) = \sum_{n=-\infty}^{\infty} e^{i\pi\tau(n+a)^2} e^{i2\pi(n+a)(z+b)}$ is the Jacobi Θ function [17].

Vortex structure. We can now compare the properties of magnetic Bloch states for the OFL and LLL. The state $\mathbf{q} = \mathbf{0}$ of the OFL exhibits, within each unit cell, a highly contrasted dip of the total density (see Fig. 2a), around which the velocity circulates (see Fig. 2b). A similar behavior is found for different quasi-momentum states, albeit with a different hole position. This behavior strongly resembles magnetic Bloch states of the LLL, which exhibit one quantized vortex point defect per unit cell, at which the density exactly cancels (see Fig. 2c) and around which the complex phase θ winds once by 2π . The velocity field, given by

$$\mathbf{v} = \frac{1}{m|\psi^2|} \text{Re} \left[\psi^* \left(\frac{\hbar}{i} \nabla - q\mathbf{A} \right) \psi \right] = \frac{\hbar}{m} \nabla\theta - \frac{q\mathbf{A}}{m},$$

is shown in Fig. 2d. We note that the circulation of velocity around each unit cell cancels due to the compensation between the singular contribution of the vortex and

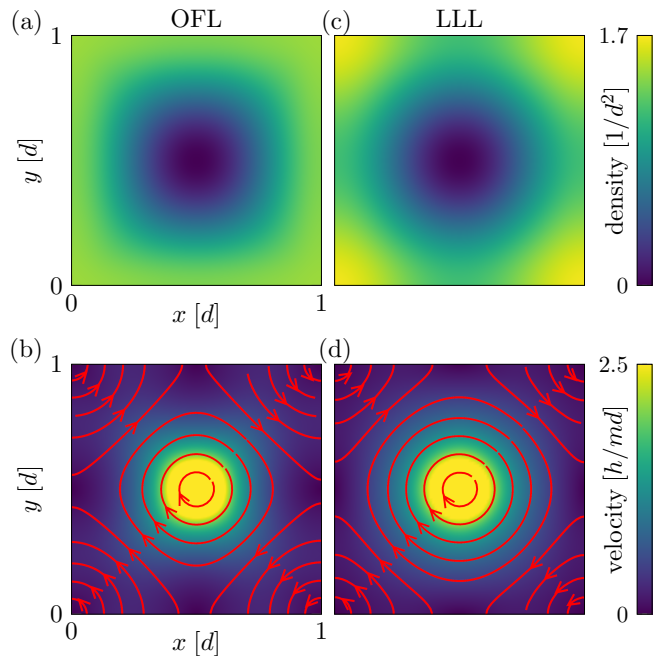


FIG. 2. Mean density (a,c) and velocity (b,d) distributions on a square unit cell $d \times d$ threaded by one unit of magnetic flux quantum. We assume a Bloch state $\mathbf{q} = \mathbf{0}$, which exhibits a quantized vortex at $(d/2, d/2)$. The left (resp. right) panels correspond to the lowest band of the OFL for $V_0 = 100 \hbar\omega_c$ (resp. the LLL). In (b,d), the color encodes the norm of the velocity, and the red arrows the velocity streamlines.

the rotational flow induced by the magnetic field. Each magnetic Bloch state thus exhibits non-zero local currents within the magnetic unit cell, but no global flow on larger length scales. The occurrence of vortices in OFL orbitals provides another illustration of the ‘ideal’ Chern band character: like in the LLL, OFL orbitals can be fully characterized by the location of quantum vortices [13].

Topological signatures with quantum gases. We now consider experimental signatures of the topological character of the low-energy bands of the OFL. We first consider a low-temperature Fermi gas in a harmonic trap $U(\mathbf{r})$ and subjected to the flux lattice. We show in Fig. 3a the total density variation of a Fermi sea, defined by a chemical potential μ_0 that is set inside the energy gap separating the ground and first excited band. It can be analysed within the local density approximation, which considers the system at position \mathbf{r} as locally homogeneous with a chemical potential $\mu(\mathbf{r}) = \mu_0 - U(\mathbf{r})$. In the central disk defined by $\mu(\mathbf{r})$ higher than the ground band energy, the Fermi sea forms a band insulator, with a uniform coarse-grained density (see Fig. 3c). Outside this disk, the density drops to zero, and the system develops on the edge a chiral current consistent with the bulk-edge correspondence (see Fig. 3b) [18, 19].

We also consider a Bose-Einstein condensate prepared in similar conditions, in the presence of weak repulsive

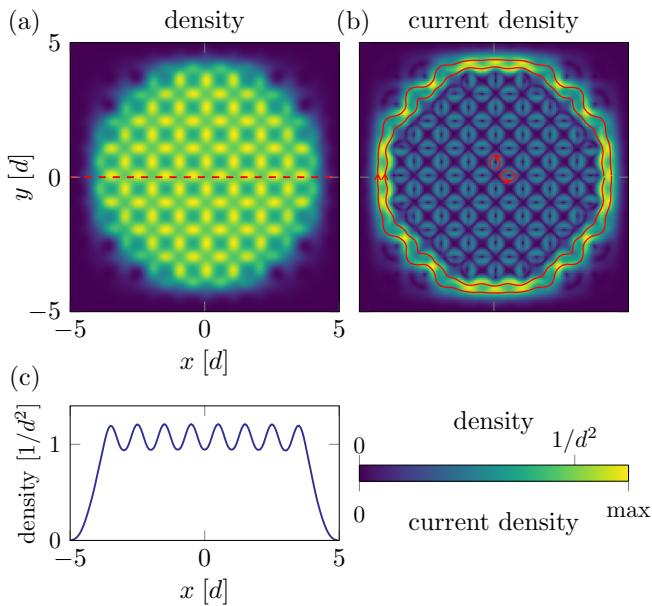


FIG. 3. In situ density (a) and current density (b) profile of a Fermi gas at zero temperature in a quasi-2D geometry subjected to the optical flux lattice with $V_0 = 100 \hbar\omega_c$ and to an isotropic harmonic trap (trapping frequency $\omega_{\text{trap}} = 0.025 \omega_c$). We used a chemical potential $\mu_0 = 1.11 \hbar\omega_c$ located between the ground and first excited bands. A few stream lines are shown as red lines in (b). (c) Density profile along the line $y = 0$, showing incompressibility in the bulk.

interactions. The condensate wavefunction is computed by evolving the Gross-Pitaevskii equation in imaginary time using a split-step method. The in situ density profile, shown in Fig. 4a, exhibits a square lattice of density holes corresponding to the regular array of quantized vortices expected for the quasi-momentum $\mathbf{q} = \mathbf{0}$. We point that, in our calculation, interactions are strong enough to significantly promote atoms to the first excited band (chemical potential $\mu \simeq 1.62 \hbar\omega_c$), which leads to a reduction of the vortex core size compared to the state $\mathbf{q} = \mathbf{0}$ of the ground band, shown in Fig. 2a.

This vortex lattice shares similarities with those observed in rotating Bose gases [20–22], albeit arranged here on a square lattice imposed by the OFL geometry. In practice, vortices can be first revealed as holes in the density profile [23]. One can also consider observing them after a time-of-flight expansion in order to magnify them and reveal the associated quantized phase winding. In our flux lattice implementation, the velocity distribution cannot be used as such to reveal the vortex lattice, because it only expands over several discrete Bragg peaks (see Fig. 4b) [24]. On the other hand, it was shown in [25] that any state of the lowest Landau level in the symmetric gauge expands in time-of-flight in a self-similar manner. In order to retrieve the vortex lattice configuration in time-of-flight, the condensate wavefunction should be multiplied by the factor $\exp(i\pi xy/d^2)$ corresponding

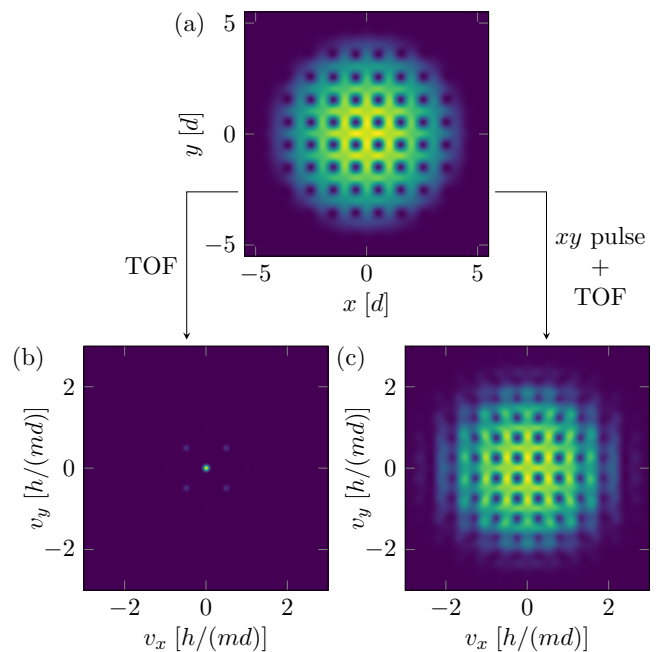


FIG. 4. (a) In situ density profile of a Bose-Einstein condensate in a quasi-2D geometry subjected to the optical flux lattice with $V_0 = 100 \hbar\omega_c$ and to an isotropic harmonic trap. We used a trapping frequency $\omega_{\text{trap}} = 0.1 \omega_c$ and an interaction coupling constant g such that $gN/d^2 = 100 \hbar\omega_c$, where N is the number of atoms per spin state. (b) Velocity distribution obtained after a free expansion. The discrete Bragg peaks do not contain information on the vortex lattice structure prior expansion. (c) Velocity distribution obtained after a short pulse of quadrupolar potential Qxy mapping the condensate wavefunction to the symmetric gauge. In that case, velocity distribution reveals the vortex lattice structure.

to the gauge transform from the Landau to symmetric gauge, which can be performed by apply a quadrupolar potential Qxy for a short duration prior to expansion. This is confirmed by calculating the velocity distribution of the condensate wavefunction multiplied by the complex phase factor (see Fig. 4c).

Implementation. Different optical setups can be envisioned for implementing the proposed OFL. Since it involves a polarization pattern sitting in the plane xy , a first possibility is to use light beams propagating along z , with a spatial structure controlled by a spatial light modulators [26]. This configuration allows fine tuning of the polarization landscape, at the expense a limited spatial resolution. Another possible scheme involves laser beams propagating solely in the xy plane, which typically leads to smaller unit cells, hence larger cyclotron frequencies. We present in appendix 3 such a planar laser configuration with a triangular symmetry. This dark-state OFL gives rise to similar Landau-level-like dynamics, and one expects Bose-Einstein condensates in this structure to form a triangular vortex lattice.

We also considered the effect of imperfect realization

of the atom-laser coupling geometry and the influence of a residual magnetic field on the band structure. As discussed in appendix 4, fine tuning of these parameters can be used to flatten the ground band dispersion, and topological features are robust with respect to moderate uncontrolled imperfections.

In conclusion, we have proposed a generalization of optical flux lattices to a dark internal state of an atom. This scheme gives rise to continuum topological bands even in the presence of a strong optical lattice. Those bands can be described as ‘ideal’ Chern bands to a very good approximation, so that they inherit the algebraic structure of Landau levels. As shown in [12], this property guarantees the existence of many-body ground states described by model wavefunctions, such as the bosonic Laughlin state at half filling. This, combined with the strong reduction of spontaneous emission in dark internal states, makes our proposal appealing for the simulation of quantum Hall effect in atomic gases.

We acknowledge insightful discussions with Raphael Lopes, Jérôme Beugnon, Nathan Goldman and Zoran Hadzibabic. This research was funded by European Union (grant TOPODY 756722 from the European Research Council), Institut Universitaire de France, and Agence Nationale de la Recherche (ANR), projects ANR-24-CE30-7961 and ANR-24-CE47-2670-01.

* sylvain.nascimbene@lkb.ens.fr

† jean.dalibard@lkb.ens.fr

- [1] N. R. Cooper, J. Dalibard, and I. B. Spielman, Topological bands for ultracold atoms, *Rev. Mod. Phys.* **91**, 015005 (2019).
- [2] T. Ozawa, H. M. Price, A. Amo, N. Goldman, M. Hafezi, L. Lu, M. C. Rechtsman, D. Schuster, J. Simon, O. Zeitlinger, and I. Carusotto, Topological photonics, *Rev. Mod. Phys.* **91**, 015006 (2019).
- [3] N. R. Cooper, Optical Flux Lattices for Ultracold Atomic Gases, *Phys. Rev. Lett.* **106** (2011).
- [4] G. Juzeliūnas and I. B. Spielman, Flux lattices reformulated, *New J. Phys.* **14**, 123022 (2012).
- [5] N. R. Cooper and J. Dalibard, Reaching Fractional Quantum Hall States with Optical Flux Lattices, *Phys. Rev. Lett.* **110**, 185301 (2013).
- [6] H. Miyake, G. A. Siviloglou, C. J. Kennedy, W. C. Burton, and W. Ketterle, Realizing the Harper Hamiltonian with Laser-Assisted Tunneling in Optical Lattices, *Phys. Rev. Lett.* **111**, 185302 (2013).
- [7] M. Aidelsburger, M. Atala, M. Lohse, J. T. Barreiro, B. Paredes, and I. Bloch, Realization of the Hofstadter Hamiltonian with Ultracold Atoms in Optical Lattices, *Phys. Rev. Lett.* **111**, 185301 (2013).
- [8] G. Jotzu, M. Messer, R. Desbuquois, M. Lebrat, T. Uehlinger, D. Greif, and T. Esslinger, Experimental realization of the topological Haldane model with ultracold fermions, *Nature* **515**, 237 (2014).
- [9] R. Dum and M. Olshani, Gauge Structures in Atom-Laser Interaction: Bloch Oscillations in a Dark Lattice, *Phys. Rev. Lett.* **76**, 1788 (1996).
- [10] C. Cohen-Tannoudji, J. Dupont-Roc, and G. Grynberg, *Atom-Photon Interactions: Basic Processes and Applications* (John Wiley & Sons, 1998).
- [11] R. Roy, Band geometry of fractional topological insulators, *Phys. Rev. B* **90**, 165139 (2014).
- [12] J. Wang, J. Cano, A. J. Millis, Z. Liu, and B. Yang, Exact Landau Level Description of Geometry and Interaction in a Flatband, *Phys. Rev. Lett.* **127**, 246403 (2021).
- [13] P. J. Ledwith, A. Vishwanath, and D. E. Parker, Vortexability: A unifying criterion for ideal fractional Chern insulators, *Phys. Rev. B* **108**, 205144 (2023).
- [14] B. Estienne, N. Regnault, and V. Crépel, Ideal Chern bands as Landau levels in curved space, *Phys. Rev. Res.* **5**, L032048 (2023).
- [15] F. D. M. Haldane, Many-Particle Translational Symmetries of Two-Dimensional Electrons at Rational Landau-Level Filling, *Phys. Rev. Lett.* **55**, 2095 (1985).
- [16] F. D. M. Haldane and E. H. Rezayi, Periodic Laughlin-Jastrow wave functions for the fractional quantized Hall effect, *Phys. Rev. B* **31**, 2529 (1985).
- [17] N. Read and E. Rezayi, Quasiholes and fermionic zero modes of paired fractional quantum Hall states: The mechanism for non-Abelian statistics, *Phys. Rev. B* **54**, 16864 (1996).
- [18] B. I. Halperin, Quantized Hall conductance, current-carrying edge states, and the existence of extended states in a two-dimensional disordered potential, *Phys. Rev. B* **25**, 2185 (1982).
- [19] Y. Hatsugai, Chern number and edge states in the integer quantum Hall effect, *Phys. Rev. Lett.* **71**, 3697 (1993).
- [20] K. W. Madison, F. Chevy, W. Wohlleben, and J. Dalibard, Vortex formation in a stirred Bose-Einstein condensate, *Phys. Rev. Lett.* **84**, 806 (2000).
- [21] J. R. Abo-Shaeer, C. Raman, J. M. Vogels, and W. Ketterle, Observation of vortex lattices in Bose-Einstein condensates, *Science* **292**, 476 (2001).
- [22] V. Schweikhard, I. Coddington, P. Engels, V. P. Mosenfelder, and E. A. Cornell, Rapidly Rotating Bose-Einstein Condensates in and near the Lowest Landau Level, *Phys. Rev. Lett.* **92** (2004).
- [23] B. Mukherjee, A. Shaffer, P. B. Patel, Z. Yan, C. C. Wilson, V. Crépel, R. J. Fletcher, and M. Zwierlein, Crystallization of bosonic quantum Hall states in a rotating quantum gas, *Nature* **601**, 58 (2022).
- [24] S. K. Baur and N. R. Cooper, Adiabatic preparation of vortex lattices, *Phys. Rev. A* **88**, 033603 (2013).
- [25] N. Read and N. R. Cooper, Free expansion of lowest-Landau-level states of trapped atoms: A wave-function microscope, *Phys. Rev. A* **68**, 035601 (2003).
- [26] C. Rosales-Guzmán, N. Bhebhe, and A. Forbes, Simultaneous generation of multiple vector beams on a single SLM, *Opt. Express* **25**, 25697 (2017).
- [27] M. A. Olshani and V. G. Minogin, Three-dimensional velocity-selective coherent population trapping of a (3+3)-level atom, *Optics Communications* **89**, 393 (1992).

Appendices

1. Dark state of a $J_g = 1 \leftrightarrow J_e = 1$ transition

In this Letter, we consider the atomic transition sketched in figure 5, connecting the ground electronic level to an excited level, both with unit angular momentum. We indicate in the figure the values of the constant factors (derived from Clebsch-Gordan coefficients) entering in the calculation of the coupling between a Zeeman state $|g, m\rangle$ of the ground level and the Zeeman state $|e, m' = 0\rangle$ of the excited level. Since the coupling factor between the states $|g, 0\rangle$ and $|e, 0\rangle$ is null, an atom initially prepared in the subspace $\{|g, \pm 1\rangle, |e, 0\rangle\}$ will remain in this subspace if the light field only contains left- and right-handed circular polarizations.

Suppose now that the light field is monochromatic with a frequency ω_L larger than the resonance frequency ω_A . Suppose also that the one-photon couplings $\kappa_{m,0}^{(ge)}$ and $\kappa_{0,m}^{(eg)} = [\kappa_{m,0}^{(ge)}]^*$ between the Zeeman ground states $|g, m = \pm 1\rangle$ and the Zeeman excited state $|e, 0\rangle$ is at any point \mathbf{r} much smaller than the detuning $\Delta = \omega_L - \omega_A$. One can then restrict the internal atomic dynamics to the ground states $|g, \pm 1\rangle$ manifold by introducing the two-photon Rabi frequencies

$$\kappa_{m_1, m_2}^{(gg)} = \frac{\kappa_{m_1, 0}^{(ge)} \kappa_{0, m_2}^{(eg)}}{\Delta}. \quad (4)$$

This leads to the 2×2 matrix $V(\mathbf{r})$ used in the main text [eq.(1)].

In practice, a transition $J_g = 1 \leftrightarrow J_e = 1$ can be isolated for different alkali atoms, such as ${}^7\text{Li}$, ${}^{39}\text{K}$, ${}^{41}\text{K}$ and ${}^{87}\text{Rb}$. More precisely, one can use a laser close to the D1 or D2 line connecting the hyperfine levels $F_g = F_e = 1$. The most favourable configuration is the D1 line of ${}^{87}\text{Rb}$, for which the considered transition is detuned with respect the nearest line connecting $F_g = 1$ to $F_e = 2$ by $\simeq 800$ MHz. Note that our scheme can be extended to any three-level system in a Λ configuration, making it relevant for a wider range of atomic gases.

We also provide the typical expected range for the cyclotron frequency ω_c . Considering ${}^{87}\text{Rb}$ atoms and the laser scheme discussed in appendix 4, with the light momentum $k = 2\pi/\lambda$ corresponding to the D1 line of wavelength $\lambda = 795$ nm, we get a cyclotron frequency $\omega_c = 2\pi \times 2.0$ kHz.

2. The non-degeneracy condition of OFLs

In its simplest version [3], an optical flux lattice (OFL) consists in a spatially periodic coupling between two internal states $|a\rangle$ and $|b\rangle$. This coupling can be written $\hat{V} = \epsilon_0 \hat{1} + \epsilon_1 \mathbf{n} \cdot \hat{\boldsymbol{\sigma}}$, where the real functions $\epsilon_0(\mathbf{r})$, $\epsilon_1(\mathbf{r})$ and the unit vector $\mathbf{n}(\mathbf{r})$ are spatially periodic, and the $\hat{\sigma}_j$ ($j = x, y, z$) are the Pauli matrices.

At any point in space, we can diagonalize \hat{V} and obtain

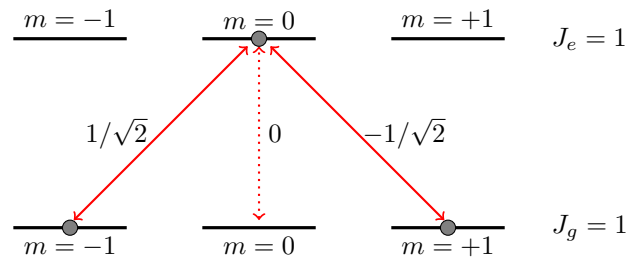


FIG. 5. Level scheme considered in this letter. An atom with a $J_g = 1 \leftrightarrow J_e = 1$ transition is irradiated by a monochromatic light field with left-handed and right-handed circular polarization components. For a proper initial state, the dynamics can be restricted to the Λ system $\{|g, \pm 1\rangle, |e, 0\rangle\}$.

the two eigenstates $|\pm\rangle_{\mathbf{n}}$ with the energies $\epsilon_0 \pm \epsilon_1$. The non-degeneracy condition stated in [3] imposes that ϵ_1 does not cancel at any point in the unit cell. Suppose for example that ϵ_1 is strictly positive everywhere, and consider the Berry connection $\mathbf{A}(\mathbf{r}) = i\hbar \mathbf{n} \cdot (-\nabla(|-\rangle_{\mathbf{n}}))$ and the Berry curvature $B_z(\mathbf{r}) = (\nabla \times \mathbf{A})_z$ that emerge for an adiabatic following of the local ground state $|-\rangle_{\mathbf{n}}$. By definition of an OFL, the flux of B_z across the unit cell should be non-zero. Using Stokes theorem, this flux is given by:

$$\iint B_z d^2r = \oint_{\mathcal{C}} \mathbf{A} \cdot d\mathbf{r} + \text{singular contributions}, \quad (5)$$

where the contour \mathcal{C} represents the edge of the unit cell. Since \mathbf{A} is periodic on the lattice, its contour integral along the cell edge is zero and one is left with only the contribution of singularities. One must therefore engineer these singularities such that their sum gives a non-zero result.

Let us choose a gauge, for example $|-\rangle_{\mathbf{n}} = (-e^{-i\phi} \sin(\theta/2), \cos(\theta/2))^T$ where the spherical angles (θ, ϕ) define the orientation of \mathbf{n} . The Berry connection then reads $\mathbf{A} = \hbar \sin^2(\theta/2) \nabla\phi$, showing that a singularity of \mathbf{A} can appear where ϕ is ill-defined. This occurs at the zeroes of the complex periodic function $V_{ab} = \epsilon_1 e^{-i\phi} \cos\theta$, hence at places where $\theta = 0$ or π . More precisely, a point where $\theta = \pi$, i.e. $V_{aa} - \epsilon_0 = \epsilon_1 \cos\theta < 0$ will lead to a singular contribution since $\mathbf{A} = \hbar \nabla\phi$ at this point, whereas \mathbf{A} will vanish at a point where $\theta = 0$, i.e. $V_{aa} - \epsilon_0 > 0$, and there will be no contribution to Eq. (5) in this case.

The theory of complex functions indicates that the zeroes of V_{ab} come by pairs, with an opposite circulation of the phase ϕ around the two zeroes of the pair. If $V_{aa} - \epsilon_0$ keeps the same sign at the location of the two zeroes, the singular contributions to Eq. (5) of the two members of the pair thus compensate each other. To obtain a non-zero flux through the unit cell of the OFL, there must be at least one pair of zeroes of V_{ab} that is "rectified", i.e.,

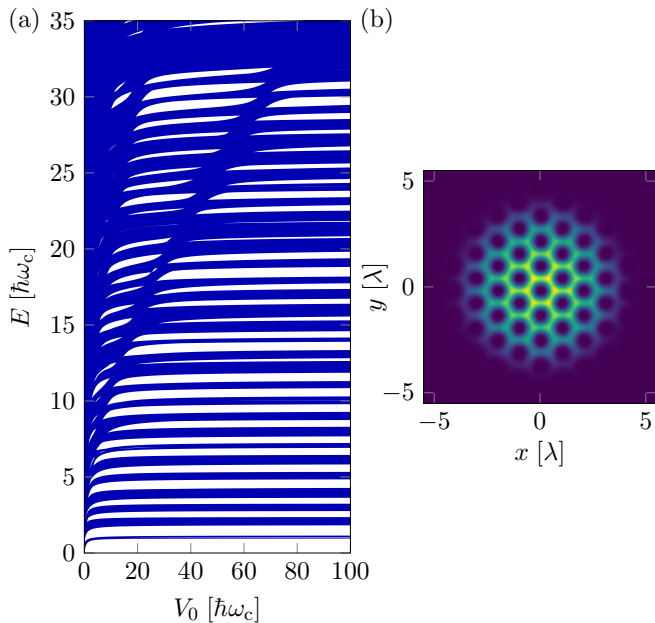


FIG. 6. (a) Bandspectrum of a dark-state OFL with a triangular symmetry, given in Eq. (8). We recognize a series of almost equally-spaced bands at low energy, akin to Landau levels. (b) Density profile of a Bose-Einstein condensate in the OFL with triangular symmetry. We used a light shift amplitude $V_0 = 100 \hbar\omega_c$, an interaction strength $gN/\lambda^2 = 5 \hbar\omega_c$, and a harmonic trap frequency $\omega_{\text{trap}} = 0.04 \omega_c$.

for which $V_{aa} - \epsilon_0$ changes sign (hence θ switches from 0 to π) between the two pair members.

Consider now the coupling $\hat{V}(\mathbf{r})$ given in Eq. (1). The off-diagonal matrix element $V_{ab}(\mathbf{r}) = -V_0 \alpha_+(\mathbf{r}) \alpha_-^*(\mathbf{r})$ vanishes at the zeroes of the two coefficients α_{\pm} . If the zeroes of α_+ and α_- do not overlap, then the rectification described above cannot operate. All zeroes of α_+ lead to a positive sign of $V_{aa} - \epsilon_0 = V_0(|\alpha_-|^2 - |\alpha_+|^2)/2$ and their contributions to Eq. (5) thus compensate. Similarly all zeroes of α_- lead to a negative sign of $V_{aa} - \epsilon_0$, hence no contribution to Eq. (5) either: one cannot reach a non-zero flux in this case. The only way to circumvent this conclusion is to allow at least some partial overlap between the zeroes of α_+ and α_- . However in this case, \hat{V} vanishes at these common zeroes, and the two eigenstates of \hat{V} coincide. As we show in the main text, this local degeneracy does not prevent the achievement of a series of topological bands.

3. Triangular version of the dark-state lattice

We focused in the main text on a square version of the lattice. We show in this appendix that the same idea can be implemented in a triangular geometry. Consider the lattice formed by superposing three standing waves in the xy plane, with an in-plane linear polarization ϵ_i , and a σ_+ polarized running wave propagating along the z axis. All beams are assumed to have the same frequency ω and

the resulting electric field reads, up to a multiplicative constant:

$$\mathbf{E}(\mathbf{r}, t) \propto \left[\sum_{i=1}^3 \epsilon_i \cos(\mathbf{k}_i \cdot \mathbf{r}) e^{i\varphi_i} + a_0 \epsilon_+ \right] e^{-i\omega t} + \text{c.c.} \quad (6)$$

where the wave vectors \mathbf{k}_i are at 120° from each other and $\epsilon_i = \hat{\mathbf{k}}_i \times \hat{\mathbf{z}}$. The phases φ_i are chosen as $\varphi_1 = 0$, $\varphi_2 = 2\pi/3$, $\varphi_3 = 4\pi/3$ and the relative amplitude a_0 of the beam propagating along z is set at the value $a_0 = 3/2$. As for the lattice considered in the main text, the field can be decomposed on the ϵ_{\pm} basis

$$\mathbf{E}(\mathbf{r}) \propto [\alpha_+ \epsilon_+ + \alpha_- \epsilon_-] e^{-i\omega t} + \text{c.c.} \quad (7)$$

with the amplitudes α_{\pm} entering in the coupling matrix \hat{V} of Eq. (1):

$$\begin{aligned} \alpha_+ &= c_1 + c_2 + c_3 + \frac{3}{2} \\ \alpha_- &= c_1 - \frac{1}{2}(c_2 + c_3) + i\frac{\sqrt{3}}{2}(c_2 - c_3) \end{aligned} \quad (8)$$

where $c_i = \cos(\mathbf{k}_i \cdot \mathbf{r})$. The zeroes of α_- are found at two sets of points. The first one corresponds to the locations where all $c_j = 1$, the second one to the locations where all $c_j = -1/2$. The second set coincides with the locations of the zeroes of α_+ , so that the coupling matrix \hat{V} vanishes at these points. We recall that this local degeneracy is required for a dark-state based OFL (see appendix 1).

We show in Fig. 6a the energy spectrum as a function of the light coupling strength V_0 . For large enough V_0 , we find a series of almost equally-spaced energy bands, with a spacing $\hbar\omega_c = \sqrt{3}\hbar^2 k^2 / (2\pi m)$ consistent with the cyclotron frequency expected for the magnetic flux density. For $V_0 = 100 \hbar\omega_c$, we find a topological lowest band with a flatness ratio $\simeq 5$. An example of Bose-Einstein condensate with a triangular vortex lattice in this configuration is shown in Fig. 6b.

4. Topological robustness of the ground band

The lattice considered in the main text, described by Eqs. (1-3), depends only on the parameter V_0 . Moreover the low-energy band structure is essentially independent of V_0 for large values of this parameter (figure 1). We consider here the sensitivity of our results to different kinds of imperfections, namely a modification of the light field profile and an external magnetic field. More specifically, we consider light field amplitudes α_+ and α_- given by

$$\begin{aligned} \alpha_+(\mathbf{r}) &= \gamma + \frac{1}{2} [\cos(kx) + \cos(ky)], \\ \alpha_-(\mathbf{r}) &= \beta \left\{ \sin\left[\frac{k}{2}(x-y)\right] - i \sin\left[\frac{k}{2}(x+y)\right] \right\} \end{aligned} \quad (9)$$

parametrized by the parameters β and γ . We also study the influence of a magnetic field along z giving rise to a Zeeman splitting $h_z m_z$. The band structure presented in the main text correspond to the values $\beta = \gamma = 1$ and $h_z = 0$.

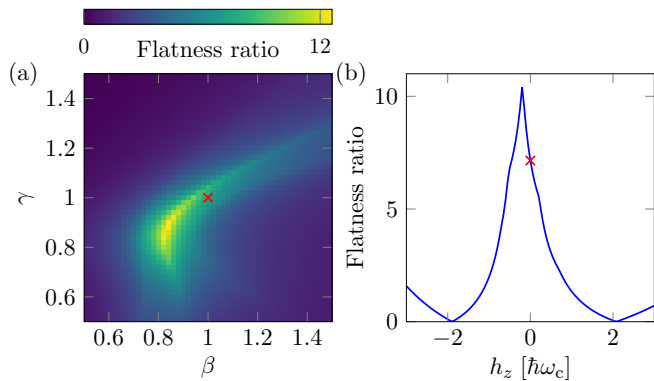


FIG. 7. (a) Evolution of the flatness ratio of the lowest band (ratio between the gap and the band width) for $V_0 = 100 \hbar\omega_c$ as a function of β and γ , for $h_z = 0$. (b) Evolution of the flatness ratio with h_z , for $\beta = \gamma = 1$. The red crosses correspond to the values $\beta = \gamma = 1$ and $h_z = 0$ considered in the main text.

We focus here on the flatness ratio of the lowest band, i.e., the ratio of the gap to the first excited band and the width of this lowest band. We plot the result in Fig. 7 for $V_0 = 100 \hbar\omega_c$. We find a non-zero flatness ratio for the whole range explored in the figure ($0.5 < \beta, \gamma < 1.5$), indicating the robustness of the topology of the lattice. Similarly, the topological character of the band is preserved for Zeeman fields $|h_z| \lesssim 2 \hbar\omega_c$. We also note that the band width can be significantly decreased with a fine tuning of the values of β and γ . For $\beta = 0.92$, $\gamma = 0.88$ and $h_z = -0.25 \hbar\omega_c$, this width is only $0.06 \hbar\omega_c$ (flatness ratio of 13.9) instead of $0.11 \hbar\omega_c$ for $\beta = \gamma = 1$ and $h_z = 0$ (flatness ratio of 7.2). This fine tuning should ease the reach of fractional quantum Hall states, for which the interaction energy dominates over the kinetic energy (i.e. the band width).

We mention that our dark-state OFL is also intrinsically robust to polarization defects, given the fact that a dark internal state can be always be defined for any monochromatic electric field at the vicinity of a $J_g = 1$ to $J_e = 1$ optical transition [27].